Quantum Deconstruction of the Infrared Spectrum of CH_5^+

Xinchuan Huang *et al.*

Science **311**, 60 (2006);
DOI: 10.1126/science.1121166

Science (print ISSN 0036-8075; online ISSN 1095-9203) is published weekly, except the last week in December, by the American Association for the Advancement of Science, 1200 New York Avenue NW, Washington, DC 20005.

seems to be the case for the one-photon transition frequency ν_{01}. This fact is also confirmed by the large quality factor that we extract from the resonant activation measurements. From Q, we derive the total shunting impedance $1/\mathrm{Re}(Y) = 4700$ ohms of the junction. This is much larger than the expected shunt impedance for a current-biased JJ, which is approximately the typical wire impedance at microwave frequencies ≈100 ohms. In this sense, the STO dielectric resonator protects the junction from its environment at the characteristic transition frequency ν_{01}.

Even though with our experiment, we are not able to determine univocally the intrinsic dissipation of the Josephson element, we can extract a lower bound. Assuming that all dissipation comes from the Josephson element, we can calculate the intrinsic impedance $1/\mathrm{Re}(Y_{\mathrm{int}})$ in parallel with the Josephson inductance. According to the circuit of Fig. 2C, we have $1/\mathrm{Re}(Y_{\mathrm{int}}) = L_J^2/(L_J + L_S)^2\mathrm{Re}(Y) \approx 700$ ohms for the lowest value of the intrinsic impedance due to low-lying energy excitations. This result may open up the possibility for some kind of freezing mechanism for quasiparticles at very low temperature and/or the existence of a subdominant imaginary s-wave component of the order parameter inducing a gapped excitation spectrum. The observation of quantum tunneling, narrow width of excited states, and a large Q value support the notion of "quiet" qubits based on d-wave symmetry superconductor.

References and Notes

1. Y. Makhlin, G. Schön, A. Shnirman, *Rev. Mod. Phys.* **73**, 357 (2001).
2. J. Clarke, A. N. Cleland, M. H. Devoret, D. Esteve, J. M. Martinis, *Science* **239**, 992 (1988).
3. J. R. Friedman, V. Patel, W. Chen, S. K. Tolpygo, J. E. Lukens, *Nature* **406**, 43 (2000).
4. A. J. Berkley *et al.*, *Science* **300**, 1548 (2003).
5. Y. Nakamura, Y. A. Pashkin, J. S. Tsai, *Nature* **398**, 786 (1999).
6. T. Duty, D. Gunnarson, K. Bladh, P. Delsing, *Phys. Rev. B* **69**, 140503 (2004).
7. D. Vion *et al.*, *Science* **296**, 886 (2002).
8. J. M. Martinis, S. Nam, J. Aumentado, C. Urbina, *Phys. Rev. Lett.* **89**, 117901 (2002).
9. I. Chiorescu, Y. Nakamura, C. J. P. M. Harmans, J. E. Mooij, *Science* **299**, 1869 (2003).
10. T. Yamamoto, Y. A. Pashkin, O. Astafiev, Y. Nakamura, J. S. Tsai, *Nature* **425**, 941 (2003).
11. C. C. Tsuei, J. R. Kirtley, *Rev. Mod. Phys.* **72**, 969 (2000).
12. L. B. Ioffe, V. B. Geshkenbein, M. V. Feigel'man, A. L. Fauchère, G. Blatter, *Nature* **398**, 679 (1999).
13. G. Blatter, V. B. Geshkenbein, L. B. Ioffe, *Phys. Rev. B* **63**, 174511 (2001).
14. A. Blais, A. M. Zagoskin, *Phys. Rev. A* **61**, 042308 (2000).
15. M. H. S. Amin *et al.*, *Phys. Rev. B* **71**, 064516 (2005).
16. M. H. S. Amin, A. Y. Smirnov, *Phys. Rev. Lett.* **92**, 017001 (2004).
17. Y. V. Fominov, A. A. Golubov, M. Y. Kupriyanov, *JETP Lett.* **77**, 587 (2003).
18. S. Kawabata, S. Kashiwaya, Y. Asano, Y. Tanaka, *Phys. Rev. B* **72**, 052506 (2005).
19. M. Tinkham, *Introduction to Superconductivity* (McGraw-Hill International Editions, New York, ed. 2, 1996).
20. A. O. Caldeira, A. J. Leggett, *Phys. Rev. Lett.* **46**, 211 (1981).
21. M. H. Devoret *et al.*, in *Quantum Tunneling in Condensed Media*, Y. Kagan, A. J. Leggett, Eds. (North-Holland, Amsterdam, 1992), chap. 6.
22. T. Bauch *et al.*, *Phys. Rev. Lett.* **94**, 087003 (2005).
23. F. M. Granozio *et al.*, *Phys. Rev. B* **67**, 184506 (2003).
24. F. Lombardi *et al.*, *Phys. Rev. Lett.* **89**, 207001 (2002).
25. R. C. Neville, B. Hoeneisen, C. A. Mead, *J. Appl. Phys.* **43**, 2124 (1972).
26. G. Burkard, D. P. DiVincenzo, P. Bertet, I. Chiorescu, J. E. Mooij, *Phys. Rev. B* **71**, 134504 (2005).
27. T. A. Fulton, L. N. Dunkleberger, *Phys. Rev. B* **9**, 4760 (1974).
28. A. Wallraff, T. Duty, A. Lukashenko, A. V. Ustinov, *Phys. Rev. Lett.* **90**, 037003 (2003).
29. J. M. Martinis, M. H. Devoret, J. Clarke, *Phys. Rev. B* **35**, 4682 (1987).
30. J. M. Martinis ***et al.***, available at http://xxx.lanl.gov/abs/cond-mat/0507622 (2005).
31. C. C. Homes *et al.*, *Phys. Rev. B* **71**, 184515 (2005).

32. This work has greatly benefited from direct inputs from S. Kubatkin. We thank the Walther-Meissner Institut for technical support. Partly supported by the European Project Quantum Complex Systems, the Swedish Foundation for International Cooperation in Research and Higher Education International Grant 2004-2075, the Swedish Foundation for Strategic Research, and the Swedish Research Council.

30 September 2005; accepted 22 November 2005
10.1126/science.1120793

Quantum Deconstruction of the Infrared Spectrum of CH_5^+

Xinchuan Huang,[1] Anne B. McCoy,[2]* Joel M. Bowman,[1]* Lindsay M. Johnson,[2] Chandra Savage,[3] Feng Dong,[3] David J. Nesbitt[3]*

We present two quantum calculations of the infrared spectrum of protonated methane (CH_5^+) using full-dimensional, ab initio–based potential energy and dipole moment surfaces. The calculated spectra compare well with a low-resolution experimental spectrum except below 1000 cm^{-1}, where the experimental spectrum shows no absorption. The present calculations find substantial absorption features below 1000 cm^{-1}, in qualitative agreement with earlier classical calculations of the spectrum. The major spectral bands are analyzed in terms of the molecular motions. Of particular interest is an intense feature at 200 cm^{-1}, which is due to an isomerization mode that connects two equivalent minima. Very recent high-resolution jet-cooled spectra in the CH stretch region (2825 to 3050 cm^{-1}) are also reported, and assignments of the band origins are made, based on the present quantum calculations.

The CH_5^+ cation was brought to the forefront of scientific interest by a range of experimental studies (*1*–*8*) and ab initio electronic structure calculations at the stationary points (*9*–*14*) that hinted at a very high degree of fluxionality owing to the unusual two-electron–three-center bonding. The large-amplitude motions displayed by CH_5^+, even in its ground state, have made spectral assignments challenging, as is evidenced by the unassigned spectrum of Oka and co-workers (*7*). Recently, a low-resolution laser-induced reaction (LIR) infrared (IR) action spectrum of CH_5^+ was reported by Asvany *et al.* (*1*). This spectrum was recorded at 110 K over a large spectral range, 540 to 3250 cm^{-1}. The LIR spectrum is a major step forward in unraveling the dynamics of this cation.

Until very recently, dynamical studies of CH_5^+ have been hampered by the lack of a full-dimensional potential energy surface (PES). Such surfaces have just appeared and have been used in a variety of classical and quantum diffusion Monte Carlo (DMC) calculations of the ground state of CH_5^+ and its isotopomers (*15*–*19*). Thus, dynamics and vibrational calculations before 2004 were carried out in a direct fashion, that is, calculating the potential and gradients "on the fly" (*20*–*23*). These pioneering calculations were done using fairly low-level density functional theory (DFT) calculations; nevertheless, they provided great insight into the fluxional nature of CH_5^+. Indeed classical, direct-dynamics DFT simulations of the IR spectrum were also reported in (*1*) at 50 and 300 K. The 300 K spectrum is in good qualitative agreement with experiment above 1000 cm^{-1}. Below 1000 cm^{-1}, intense absorption was seen in the classical spectrum but not in the experimental one, perhaps because of a lack of experimental sensitivity in that spectral region. However, it is well known that, except in the harmonic limit, classical spectra can differ substantially from quantum spectra because of the lack of quantization in the classical dynamics. Thus, while the agreement between the classical and LIR spectra above 1000 cm^{-1} was gratifying, the differences below 1000 cm^{-1} remain an open issue.

[1]Department of Chemistry and Cherry L. Emerson Center for Scientific Computing, Emory University, Atlanta, GA 30322, USA. [2]Department of Chemistry, The Ohio State University, Columbus, OH 43210, USA. [3]JILA, National Institute of Standards and Technology, and Department of Chemistry and Biochemistry, University of Colorado, Boulder, CO 80309–0040, USA.

*To whom correspondence should be addressed. E-mail: mccoy@chemistry.ohio-state.edu (A.B.M.); jmbowma@emory.edu (J.M.B.); djn@jila.colorado.edu (D.J.N.)

Motivated by this new experimental spectrum, we undertook two quantum approaches to calculate and deconstruct the LIR spectrum using the best techniques available. In this work, we make use of a new (nonglobal), full-dimensional potential energy surface (*19*) based on the accurate coupled-cluster method [CCSD(T)] with the aug-cc-pVTZ basis and the previous MP2-based dipole moment surface (*15*). We refer to these potential and dipole moment surfaces as the CCSD(T)-MP2 surfaces. Even with these surfaces, "exact" quantum calculations of the IR spectrum are beyond reach because of the highly fluxional nature and the high dimensionality (12 internal degrees of freedom) of the CH_5^+ wave functions.

Two low-lying saddle points are the bottlenecks to the fluxional, isomerizing motion of CH_5^+. The structures and energies of the stationary points are depicted in Fig. 1. These two saddle points, and the 120 equivalent minima they connect, govern the short-time dynamics of the isomerization and, from well-known quantum time-energy relations, determine the IR spectrum under low resolution. Because our goal is to deconstruct the low-resolution LIR spectrum, we focus our quantum calculations on the minimum and these two saddle points. In one set of calculations, we perform double-harmonic (HO) calculations of the IR spectrum at these three stationary points, using the CCSD(T)-MP2 surfaces. We then weight the combined results by using the ground-state density obtained from a rigorous quantum DMC calculation (*24*). A second set of calculations was performed with the code MULTIMODE (MM), which uses variational configuration interaction methods to obtain vibrational energies and wave functions of polyatomic molecules. The code also uses an n-mode representation (nMR) of the potential that permits application to fairly large molecules (*25*). Properties such as the IR spectrum can be obtained with these wave functions; recently, this code and DMC calculations were used to stimulate the IR spectrum of $H_5O_2^+$ (*26*). In the present calculations, the single-reference version of MM is used with a four-mode representation of the potential to obtain the spectra. Higher level 5MR calculations of the vibrational eigenvalues were also performed to check the convergence of the 4MR calculations (*27*). The reference geometries for the calculations are the global minimum and the two saddle points, the same geometries used in the HO calculations, depicted in Fig. 1.

In Fig. 2, we present the stick spectra from the HO calculations and the MM calculations at the three stationary points, as well as a Gaussian convolution with full-width–half-maximum (FWHM) of 200 cm^{-1}. This width was chosen to approximate the resolution of the experimental spectrum. Both spectra have features that span the entire spectral range shown, but with no features in the 1800 to 2100 cm^{-1} range. There are quantitative differences between the spectra, with the MM spectrum showing more lines and spectral features somewhat red-shifted relative to HO spectra, as expected. In the case of the latter, each stick corresponds to a harmonic normal mode at the corresponding stationary point. For these plots, we only include the modes with real frequencies. Consequently, only 11 features are seen in the spectra at the C_{2v} and C_s(II) saddle points, because in these cases one of these frequencies becomes imaginary, whereas all 12 modes are used to construct the spectrum at the C_s(I) minimum.

These imaginary frequency modes appear as real excitations in the MM spectra. For example, at the C_{2v} saddle point reference geometry, the fundamental associated with the imaginary frequency mode is found at 200 cm^{-1} and has the greatest intensity of all the spectral lines in this spectrum. Comparison of the MM spectra at the three reference geometries shows that they are similar, especially those obtained using the C_{2v} and C_s(I) reference geometries. If these MM calculations were exact, the spectra from all three reference geometries would be identical. They are similar, but not the same, and one way to distinguish among them is to compare the zero-point energies with the exact one, obtained from DMC simulations. On the basis of this comparison (*27*), the C_{2v} reference geometry would be the preferred one. This might also be argued to be the best reference geometry because a grid centered there spans two equivalent minima and the C_s(II) saddle point. However, for comparison with experiment, we used the sum of the three MM spectra, weighted by the DMC populations at the corresponding reference geometry. Comparing the HO and MM spectra at the three stationary points, we note that there is also good overall agreement above 1000 cm^{-1}. As we noted previously (*16*), the two lowest frequency modes are very anharmonic, and differences below 1000 cm^{-1} reflect a breakdown of the HO approximation in this region.

Figure 3A shows a comparison of the calculated spectra with the experimental spectrum of Asvany *et al*. The MM and HO spectra are sums of the convoluted spectra shown in Fig. 2, weighted by the DMC ground-state density at the three stationary points. Because of the highly anharmonic nature of the low-frequency modes, the HO spectrum is only plotted for transitions above 900 cm^{-1}. There is very good agreement between the experimental and calculated spectra above 1000 cm^{-1}, with near quantitative agreement for the MM spectrum. At lower frequencies, intensity is seen both in the MM spectrum and in the HO spectra, plotted in Fig. 2A, that is not evident in the experimental one. The absence of these intense spectral features in the experiment appears to be due to the loss of sensitivity of

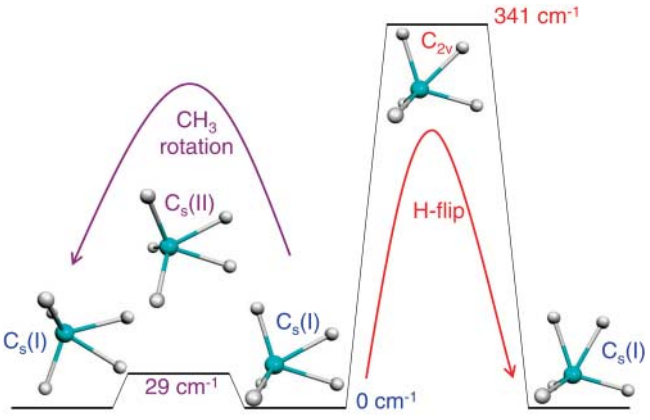

Fig. 1. Structures of CH_5^+ at the three stationary points on the potential. Energies provide the relative energies on the CCSD(T) surface.

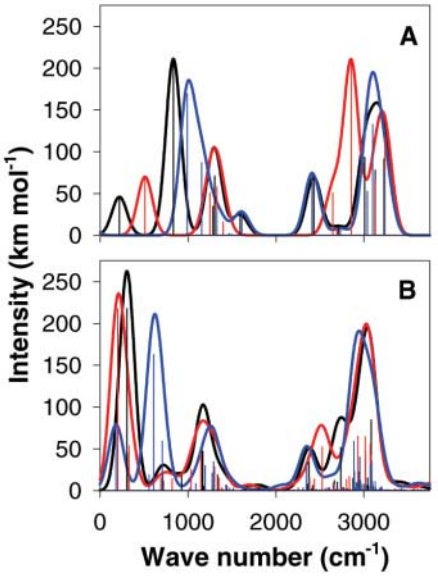

Fig. 2. Stick and Gaussian convoluted (FWHM = 200 cm^{-1}) spectra for CH_5^+ from (**A**) the double-harmonic calculations at the C_s(I) (black), C_{2v} (red), and C_s(II) (blue) stationary points and from (**B**) the MULTIMODE calculations, using the three stationary points as reference geometries. For all of these calculations, the reported intensities for the stick spectra are given in units of km mol^{-1}.

the experimental action spectrum as discussed in detail in (*1*). Interestingly, the present quantum spectra agree qualitatively with the classical one given in (*1*) in that both predict intense spectral features in this low-frequency regime. The DMC-weighted spectra agree better with experiment than any single spectrum shown in Fig. 2. This is particularly relevant for the HO spectrum and reflects the importance of all three stationary points in capturing the spectroscopy (and dynamics) of this fluxional system.

Given the good agreement with the experimental spectrum, we can assign the prominent spectral features to specific vibrations with confidence. For this analysis, we focus on the C_{2v} reference geometry, which yields several prominent features in the convoluted calculated spectra, three of which line up very well with experiment. We analyze the harmonic modes and MM wave functions that correspond to these features. For the harmonic treatment, the analysis is straightforward. For the MM wave functions, we focus on the fundamentals that provided the leading contributions to the intense bands in each spectral region. From this analysis, we find that only one or two modes provided the leading contributions to the intensity in the four regions, labeled a to d in Fig. 3A. These are depicted with the harmonic frequencies and MM energies of the corresponding major bright eigenstates in Table 1, in effect representing a quantum deconstruction of this spectrum. Feature a, the most intense one, corresponds to the imaginary frequency isomerization mode at the C_{2v} saddle point. Displacement in this coordinate brings CH_5^+ close to its geometry at a C_s(I) minimum (Table 1). Feature b reflects two modes of roughly equal intensity in the HO spectrum. These modes can be best thought of as bending or rocking motions of H_A-C-H_C and H_D-C-H_E. Finally, the large peak at high frequency (c and d) and the smaller shoulder on the red side of this feature result from CH stretching vibrations. The descriptions of all six of these modes will change if one of the other two stationary points is considered. These reflect differences in the overall symmetry of the ion; the qualitative picture, however, remains the same.

This theoretical deconstruction clearly works well in comparison with the low-resolution LIR spectra. We can also test predictions against high-resolution direct absorption spectra of jet-cooled CH_5^+ in the 2825 to 3050 cm^{-1} region that we obtained recently (*28*). Because the present theoretical study does not include rotational structure, we compare a 10 cm^{-1} convolution of both experimental and theoretical (DMC-weighted MM) spectra in Fig. 3B. Despite the simplicity of the approach, there is a very good correlation between the two largest peaks in the convoluted experimental spectrum and the accumulation of transitions near 3010 and 3075 cm^{-1} in the MM spectrum when we shift the MM spectrum by 58 cm^{-1}. The size of this shift is well within the uncertainties of the present calculations, which contain errors that arise from both the PES and the vibrational calculations. These features can be assigned to two normal-mode CH-stretch fundamentals of the CH_3^+ subunit. This simple vibrational assignment may seem surprising for such a fluxional molecule. However, if one considers a HO treatment at the three stationary points, the two highest frequency modes all correspond to stretches of the CH_3^+ subunit, with the corresponding frequencies lying in tight windows from 3097 to 3128 cm^{-1} and 3226 to 3237 cm^{-1}, respectively. Therefore, these highest frequencies appear not to be affected by the lower frequency fluxional motions of CH_5^+.

We find these comparisons extremely encouraging, but much still remains to be learned

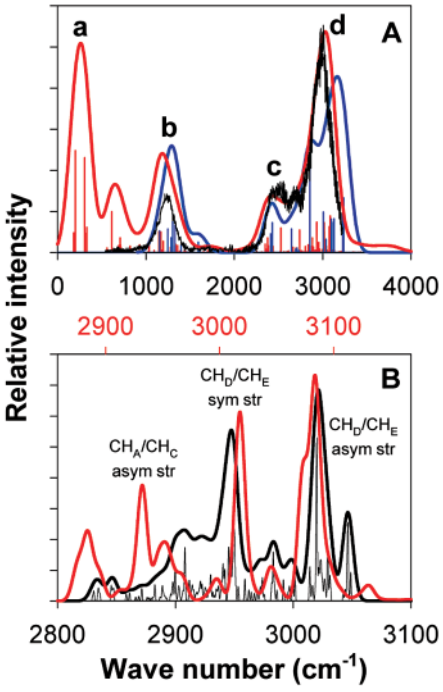

Fig. 3. Comparison of the experimental (**A**) LIR spectrum and (**B**) convoluted high-resolution spectrum and the calculated spectra of CH_5^+, with the experimental spectra plotted in black, the MULTIMODE spectra in red, and the harmonic spectrum in blue. The calculated spectra are obtained by weighting the spectra obtained at each stationary point by the probability amplitude at the stationary points and summing the spectra. For (A), the stick spectra are convoluted by a Gaussian function with FWHM = 200 cm^{-1}; in (B), the experimental spectrum is convoluted to a 1 cm^{-1} (thin line) and 10 cm^{-1} (thick line) FWHM, whereas the calculated spectrum uses a FWHM of 10 cm^{-1} and has been shifted by 58 cm^{-1} relative to the experimental spectrum, as indicated by the scaling on the top of the graph.

Table 1. Normal modes and frequencies (cm^{-1}) at the C_{2v} saddle point that contribute intensity to features a to d in Fig. 3A. Numbers in parentheses are the 5MR MULTIMODE energies (*27*) of the major eigenstate of these features obtained from the calculation at the C_{2v} reference geometry. We have used red, blue, and green to differentiate the hydrogen atoms, where atoms A and C are blue, atom B is red, and atoms D and E are green.

Feature*	Frequency†	Motion	Normal Mode Displacements‡
a	688i (175)	H_B flip	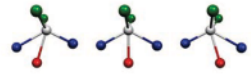
b	1246 (1116)	H_A-C-H_C bend/ H_D-C-H_E bend	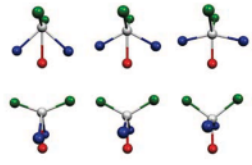
b	1328 (1293)	H_A-C-H_C rock/ H_D-C-H_E rock	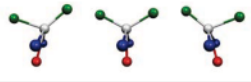 ‖
c	2854 (2468§) (2888‖)	CH_A/CH_C asymmetric stretch	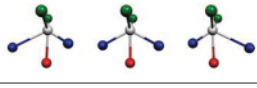
d	3121 (2983)	CH_D/CH_E symmetric stretch	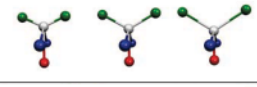
d	3237 (3067)	CH_D/CH_E asymmetric stretch	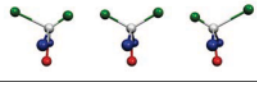

*See Fig. 3A. †Harmonic (and MULTIMODE) frequencies. ‡Pictorial depiction of the displacements. §Minor contributor to feature c, characterized as the fundamental in the CH_B stretch. ‖Mainly CH_A/CH_C asymmetric stretch, but a mixed state.

about CH_5^+ from its high-resolution spectra and accompanying rotational structure. Indeed, this is where subtle but revealing effects of the end-over-end tumbling, nuclear spin statistics, and tunneling splittings will be addressed that can not be accurately treated in the present vibrational framework (*29*, *30*). The detailed interpretation of the high-resolution spectrum of CH_5^+ and its isotopomers will clearly provide interesting opportunities for further theoretical and experimental challenges in this elusively fluxional species. Extensions of the present work to include deuterated analogs of CH_5^+ (*31*) and to probe the effects of rotations are currently under way.

References and Notes

1. O. Asvany *et al.*, *Science* **309**, 1219 (2005).
2. V. L. Tal'roze, A. K. Lyubimova, *Dokladi na Bulgarskata Akademiya na Naukite SSSR* **86**, 909 (1952).
3. K. Hiraoka, K. P. Kebarle, *J. Am. Chem. Soc.* **97**, 4179 (1975).
4. K. Hiraoka, T. Mori, *Chem. Phys. Lett.* **161**, 111 (1989).
5. R. J. Saykally, *Science* **239**, 157 (1988).
6. D. W. Boo, Z. F. Liu, A. G. Suits, J. S. Tse, Y. T. Lee, *Science* **269**, 57 (1995).
7. E. T. White, J. Tang, T. Oka, *Science* **284**, 135 (1999).
8. C. Savage, F. Dong, D. J. Nesbitt, paper presented at 60th International Symposium on Molecular Spectroscopy, Columbus, OH, 20–24 June 2005.
9. A. Olah, G. Rasul, *Acc. Chem. Res.* **30**, 245 (1997).
10. A. Komornicki, D. A. Dixon, *J. Chem. Phys.* **86**, 5625 (1987).
11. P. V. Schleyer, J. W. D. Carneiro, *J. Comput. Chem.* **13**, 997 (1992).
12. P. R. Schreiner, S. J. Kim, H. F. Schaefer, P. V. Schleyer, *J. Chem. Phys.* **99**, 3716 (1993).
13. H. Müller, W. Kutzelnigg, J. Noga, W. Klopper, *J. Chem. Phys.* **106**, 1863 (1997).
14. For a review through 2000, see (*32*).
15. A. Brown, B. J. Braams, K. Christoffel, Z. Jin, J. M. Bowman, *J. Chem. Phys.* **119**, 8790 (2003).
16. A. B. McCoy *et al.*, *J. Phys. Chem. A* **108**, 4991 (2004).
17. A. Brown, A. B. McCoy, B. J. Braams, Z. Jin, J. M. Bowman, *J. Chem. Phys.* **121**, 4105 (2004).
18. K. C. Thompson, D. L. Crittenden, M. J. T. Jordan, *J. Am. Chem. Soc.* **127**, 4954 (2005).
19. Z. Jin, B. Braams, J. M. Bowman, *J. Phys. Chem. A, Hase Festschrift Issue,* in press; appeared online as an ASAP article, 5 October 2005 doi: 10.1021/jp053848o.
20. D. Marx, M. Parrinello, *Nature* **375**, 216 (1995).
21. D. Marx, M. Parrinello, *Science* **271**, 179 (1996).
22. D. Marx, M. Parrinello, *Z. Phys. D* **41**, 253 (1997).
23. J. Tse, D. D. Klug, K. Laasonen, *Phys. Rev. Lett.* **74**, 876 (1995).
24. The quantum DMC method used in this work has been described previously [see (*16*, *17*)]. Specifically, the simulations were run for 5025, time steps of 10 atomic time units, with $\alpha = 0.1$ H. The probability amplitudes were obtained using the descendent weighting approach, counting the number of descendents of each walker after 25 time steps. To obtain the weightings used to average the spectra obtained at each of the stationary points, we calculated the probability amplitude near each of the three stationary points and averaged the results from 16 evaluations of the probability amplitudes. This yielded relative probabilities of 38% at the C_s(I) minimum, 41% at the C_{2v} saddle point, and 22% at the C_s(II) saddle point.
25. J. M. Bowman, S. Carter, X. Huang, *Int. Rev. Phys. Chem.* **22**, 533 (2003).
26. N. I. Hammer *et al.*, *J. Chem. Phys.* **122**, 244301 (2005).
27. The MULTIMODE calculations were performed in rectilinear normal modes. By including a large degree of mode-mode coupling and vibrational configuration interaction procedures, curvilinear motions are accurately described by this approach. The present calculations of the spectrum were done using a four-mode representation of the potential and CI matrices on the order of 5000 for each symmetry block (A′ and A″ for C_s calculations and A_1, A_2, B_1, and B_2 for the C_{2v} calculation). A 5MR calculation was done at the C_{2v} reference geometry, with CI matrices on the order of 15,000 for each symmetry block. The zero-point energy obtained with this large calculation is 10,989 cm^{-1}, which is close to the exact quantum DMC result of 10,908 ± 5 cm^{-1}. The 5MR energies for fundamental excitations of importance in the calculated spectrum are roughly 20 to 30 cm^{-1} lower than those from the 4MR calculations used to obtain the spectrum.
28. A more complete description of the slit discharge apparatus with application to high-resolution jet-cooled spectra of molecular ions can be found in (*33*).
29. M. P. Deskevich, D. J. Nesbitt, *J. Chem. Phys.* **123**, 084304 (2005).
30. P. R. Bunker, B. Ostojic, S. Yurchenko, *J. Mol. Struct.* **695-696**, 253 (2004).
31. X. Huang, L. M. Johnson, J. M. Bowman, A. B. McCoy, in preparation.
32. P. R. Schreiner, *Angew. Chem. Int. Ed. Engl.* **39**, 3239 (2000).
33. F. Dong, D. Uy, S. Davis, M. Child, D. J. Nesbitt, *J. Chem. Phys.* **122**, 224301 (2005).

34. We thank the authors of (*1*) for sharing experimental data, as well as D. Marx for illuminating correspondence about their classical spectral calculations. This work was supported by grants from the National Science Foundation (J.M.B., A.B.M., D.J.N.), the Office of Naval Research (J.M.B.), and the Air Force Office of Scientific Research (D.J.N.). C.S. acknowledges support from a National Research Council postdoctoral fellowship.

11 October 2005; accepted 22 November 2005
10.1126/science.1121166

Planktonic Foraminifera of the California Current Reflect 20th-Century Warming

David B. Field,[1]*† Timothy R. Baumgartner,[2] Christopher D. Charles,[1] Vicente Ferreira-Bartrina,[2] Mark D. Ohman[1]

It is currently unclear whether observed pelagic ecosystem responses to ocean warming, such as a mid-1970s change in the eastern North Pacific, depart from typical ocean variability. We report variations in planktonic foraminifera from varved sediments off southern California spanning the past 1400 years. Increasing abundances of tropical/subtropical species throughout the 20th century reflect a warming trend superimposed on decadal-scale fluctuations. Decreasing abundances of temperate/subpolar species in the late 20th century indicate a deep, penetrative warming not observed in previous centuries. These results imply that 20th-century warming, apparently anthropogenic, has already affected lower trophic levels of the California Current.

Records of various marine populations reveal that large declines in some marine algae, zooplankton, fish, and seabirds in the California Current in the late 20th century were linked to widespread ecosystem changes throughout the North Pacific in the mid-1970s (*1*–*8*). The associated change in environmental conditions resembled a sustained El Niño–like state, whereby greater cyclonic activity of the atmospheric Aleutian Low Pressure System was accompanied by warming in the eastern North Pacific (*1*–*14*). The origin of this ecosystem "regime shift" (*15*, *16*) has been a source of debate since its detection. On one hand, changes in marine populations are often attributed to decadal-scale fluctuations in ocean-atmosphere conditions that are characterized by the Pacific Decadal Oscillation (PDO) (*1*). On the other hand, the ecosystem shift could reflect penetration of a greenhouse gas–induced warming in the global ocean (*17*–*19*) that exceeded a threshold of natural variability. A major difficulty with attribution of cause is the short length of most time series of climate and ecosystem variability. The debate is further complicated by the fact that variations in many marine populations could result directly from other anthropogenic influences (such as habitat disturbance or fishing) and/or indirectly by trophic cascades. It is therefore difficult to distinguish threshold effects of a warming trend on marine populations from decadal-scale variability or other anthropogenic influences.

We present paleoceanographic evidence to show that populations of planktonic foraminifera in the California Current were strongly affected by a 20th-century warming trend. Planktonic foraminifera have been used extensively in paleoceanographic studies. They function at a low trophic level and their species-specific sensitivities to preferred hydrographic conditions link their temporal variations to changes in

[1]Scripps Institution of Oceanography, University of California, San Diego, La Jolla, CA 92093, USA. [2]Centro de Investigación Científica y de Educación Superior de Ensenada, Km 107 Carretera Tijuana-Ensenada, Ensenada, Baja California, C.P. 22860, Mexico.

*Present address: Monterey Bay Aquarium Research Institute, 7700 Sandholdt Road, Moss Landing, CA 95039, USA.

†To whom correspondence should be addressed. E-mail: dfield@mbari.org